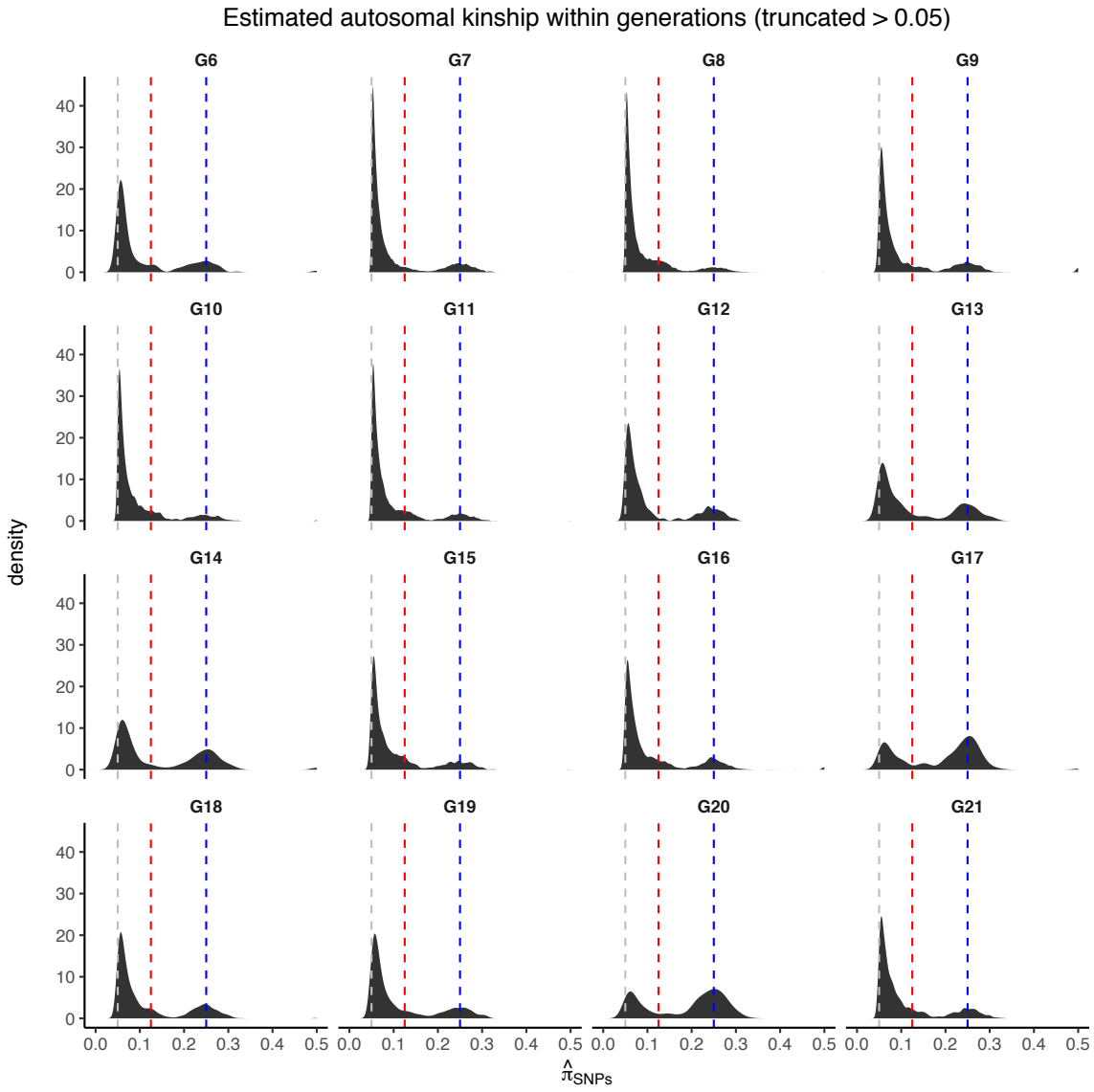

Figure S1: Distribution of relatedness within generations in the DO. Kinship coefficients estimated from autosomal SNP genotypes ($\pi_{\hat{SNPs}}$) were computed for all pairs of individuals from the same generation; only values > 0.05 are shown in order to emphasize modes in the distribution corresponding to expected values for cousins (red line; $\pi = 0.125$) and siblings (blue line; $\pi = 0.25$).

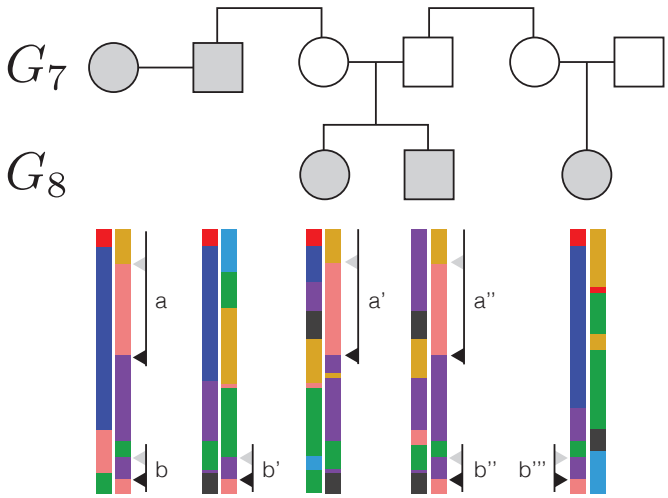

Figure S2: Joint inference of DO pedigree and sharing of crossovers. A branch of the pedigree (generations 7 and 8) inferred from SNP genotypes is shown in upper panel; filled shapes are observed individuals and open shapes unobserved. Reconstructed chromosomes are shown for each observed individual. Two focal crossovers (black arrowheads a and b) with the same position and flanking haplotypes in two or more relatives are candidates for being shared events. The presence of a neighboring crossover (grey arrowheads), also with the same position and flanking haplotypes in two or more relatives, identifies the segment (vertical bar) as shared and therefore both the focal and the neighboring crossover as shared. Thus the 14 crossovers in segments a, a', a'', a''' and b, b', b'' represent only 4 distinct crossovers shared by descent.

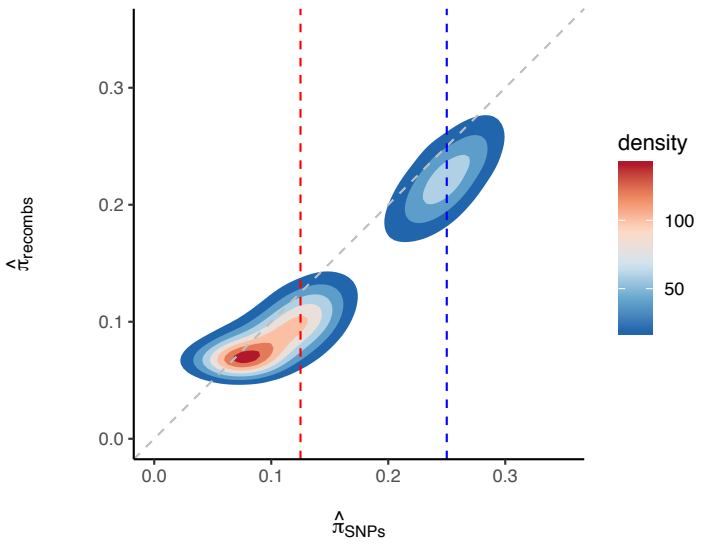

Figure S3: Comparison of kinship estimates from genotypes (x-axis) versus the proportion of non-singleton crossovers shared between individuals (y-axis). Red and blue lines represent expected kinship coefficient for cousins and siblings, respectively. Bivariate density is rendered as colors from purple (low) to orange (high). The two methods are in close agreement: Pearson's $r = 0.928$ (95% CI $0.926 - 0.929$).

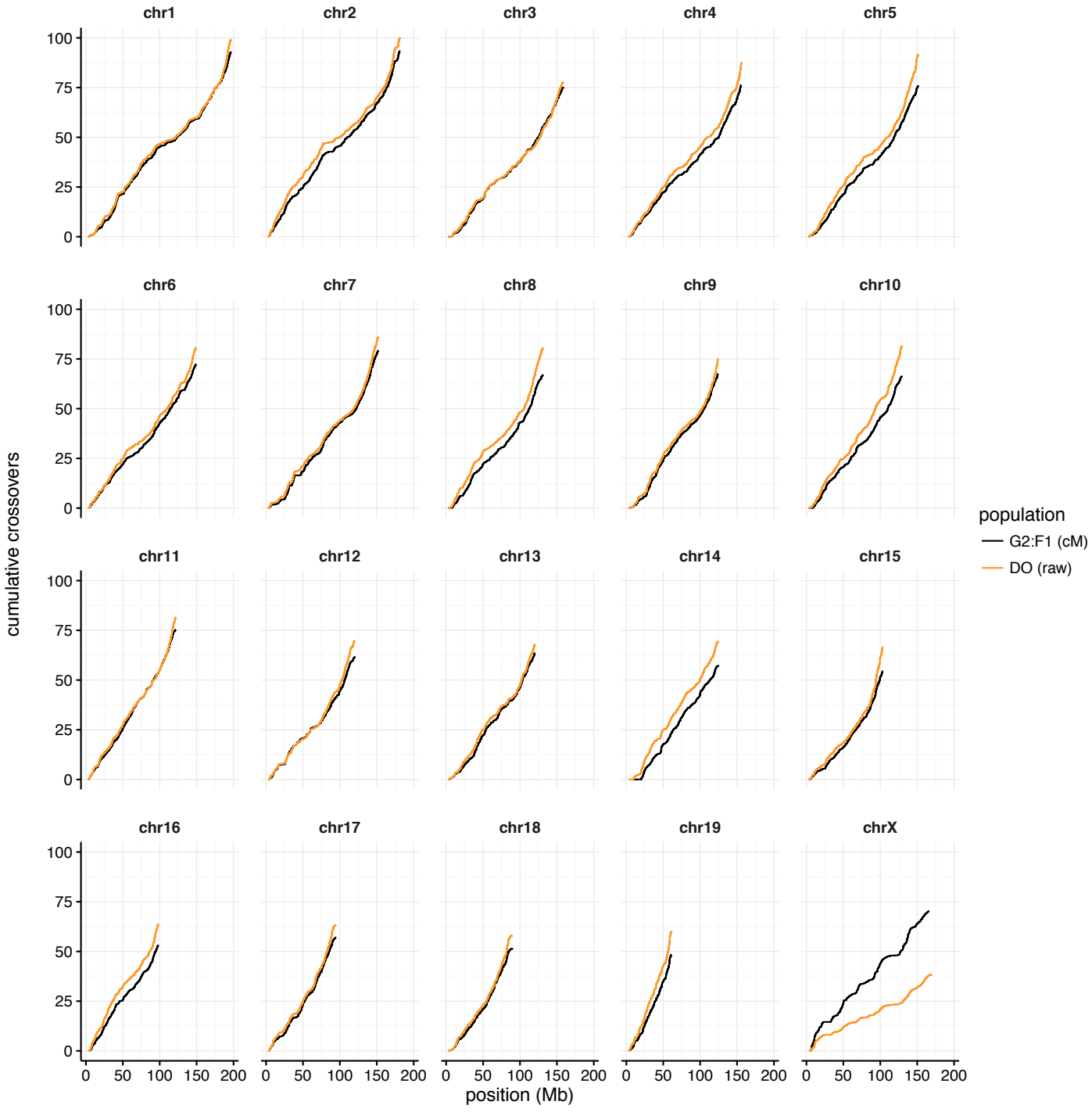

Figure S4: Comparison of cumulative recombination maps in CC and DO. Maps are shown as genetic (cM) position versus physical position (Mb) for the CC G_2:F_1 (black), and (cumulative crossover count/500) versus physical position for the DO (grey). The maps are remarkably consistent in length and shape for the autosomes, but differ in length on the X chromosome due to the increased proportion of female meioses contributing to the DO versus the CC map.

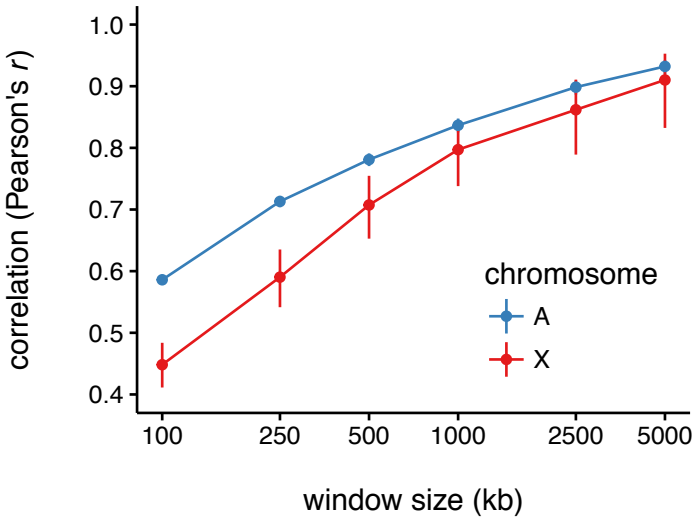

Figure S5: Correlation between DO and CC maps as a function of scale. Pearson correlation (r) between local recombination rate (measured as cM/Mb) in the DO and CC G_2:F_1, with correlations computed in windows of increasing size from 100 kb to 5 Mb. For all window sizes, rates were smoothed by allowing adjacent windows to overlap by one-half their width.

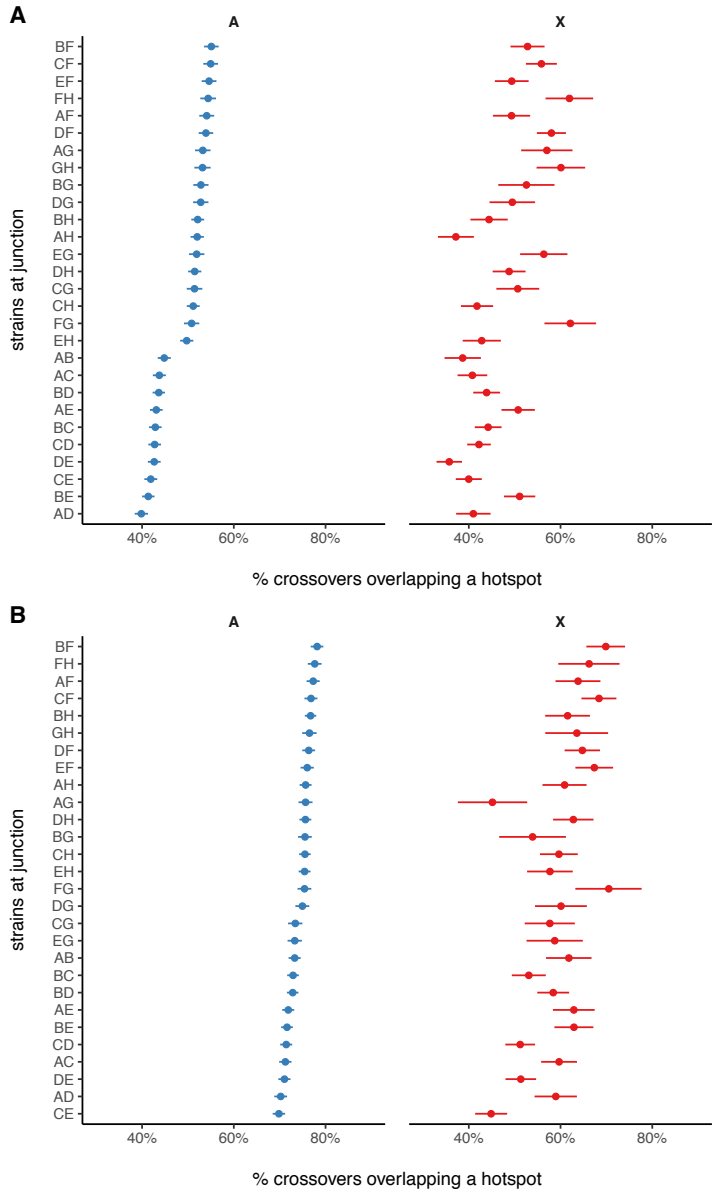

Figure S6: Recombination hotspot usage by strain pair in the DO. (**A**) Proportion of crossovers overlapping a known recombination hotspot, according to which of the $\binom{8}{2} = 28$ pairs of founder strains are present at the junction. Hotspot usage is shown separately for autosomes (A, left) and the X chromosome (X, right), and pairs are sorted according to hotspot usage on the autosomes. (**B**) Same as panel A, but only for the subset of $686,432$ crossovers refined to < 100 kb and padded to account for uncertainty in crossover localization.

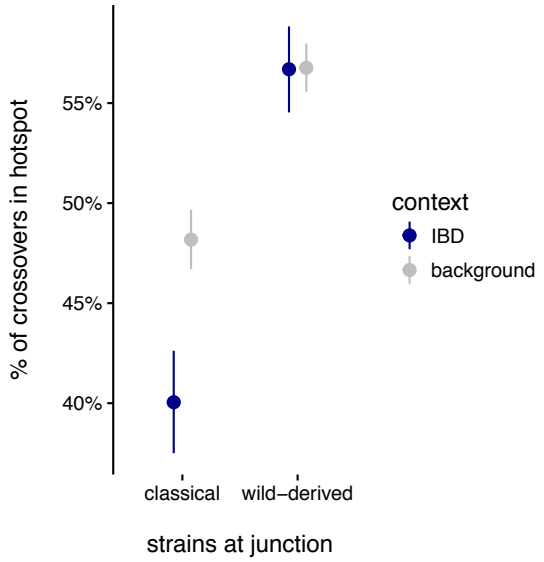

Figure S7: Proportion of crossovers overlapping a known recombination hotspot, among crossovers falling within or outside regions shared IBD between all five classical inbred founder strains.

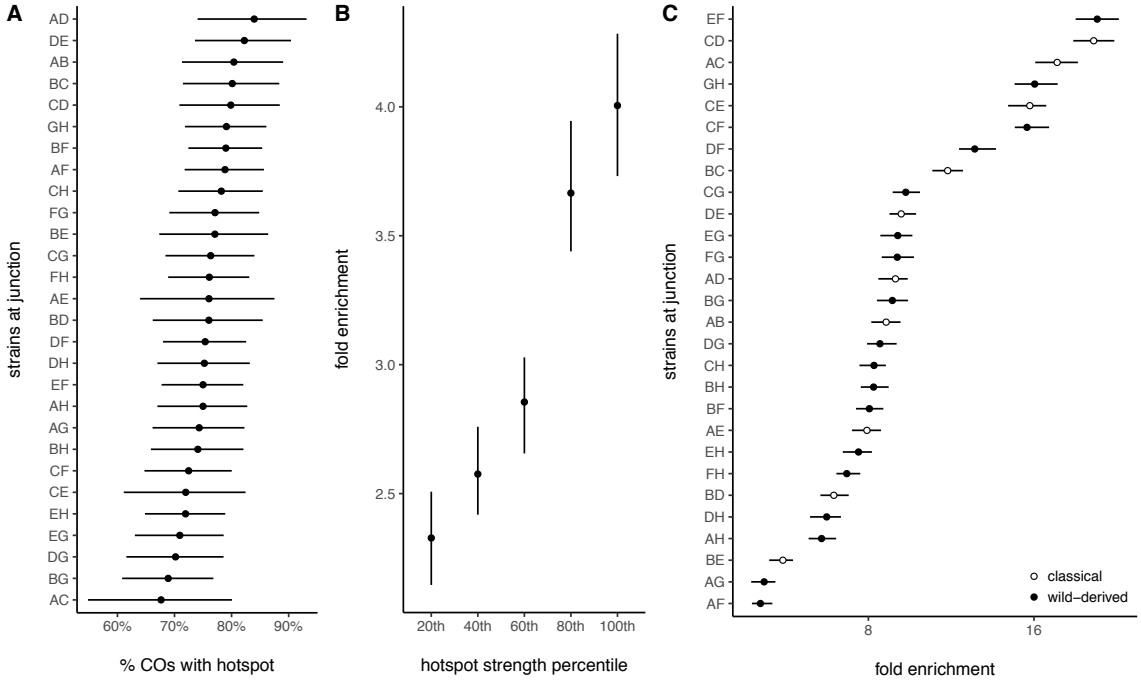

Figure S8: Utility of whole-genome sequencing for resolving crossover positions in the Collaborative Cross. (**A**) Proportion of autosomal crossovers overlapping a known recombination hotspot, according to which of the $\binom{8}{2} = 28$ pairs of founder strains are present at the junction. (**B**) Enrichment of crossover intervals for hotspots versus random genomic intervals of equal size, in five bins of hotspot strength (defined as the number of ChIP-seq reads mapped to the hotspot). (**C**) Enrichment of crossover intervals for hotspots, according to strains present at junction. Note that order of vertical axis does not match the order in panel A.

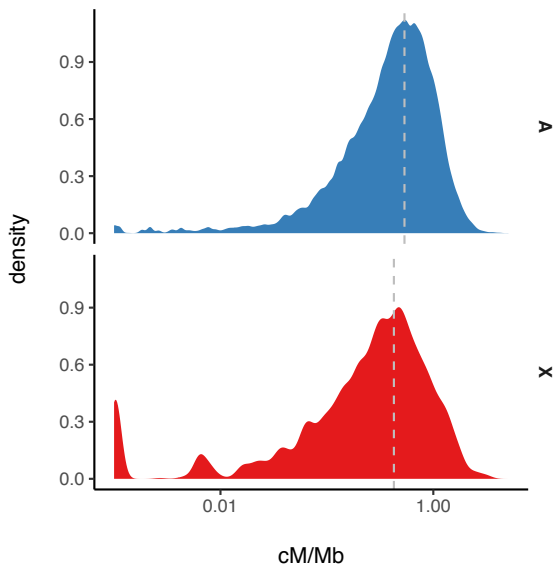

Figure S9: Distribution of local recombination rates on the autosomes and X chromosome, calculated in 500 kb windows with 100 kb offset between adjacent windows. Dashed lines indicate mean recombination rate for each chromosome type.

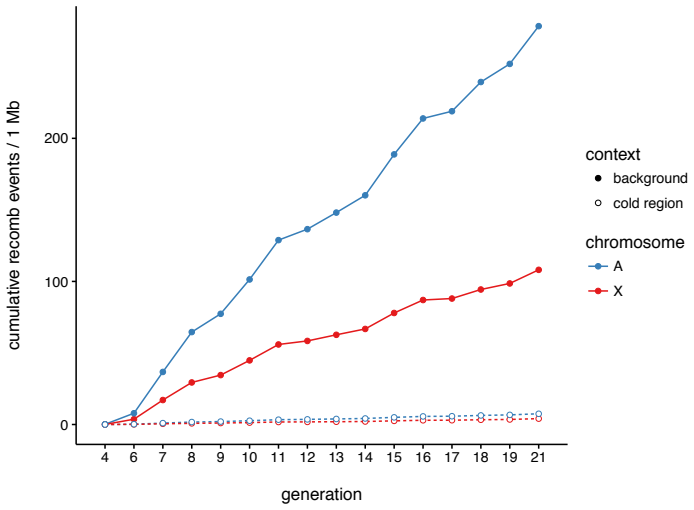

Figure S10: Accumulation of crossovers within and outside coldspots during the breeding of the DO. Autosomes (blue) and X chromosome (red) are plotted separately.

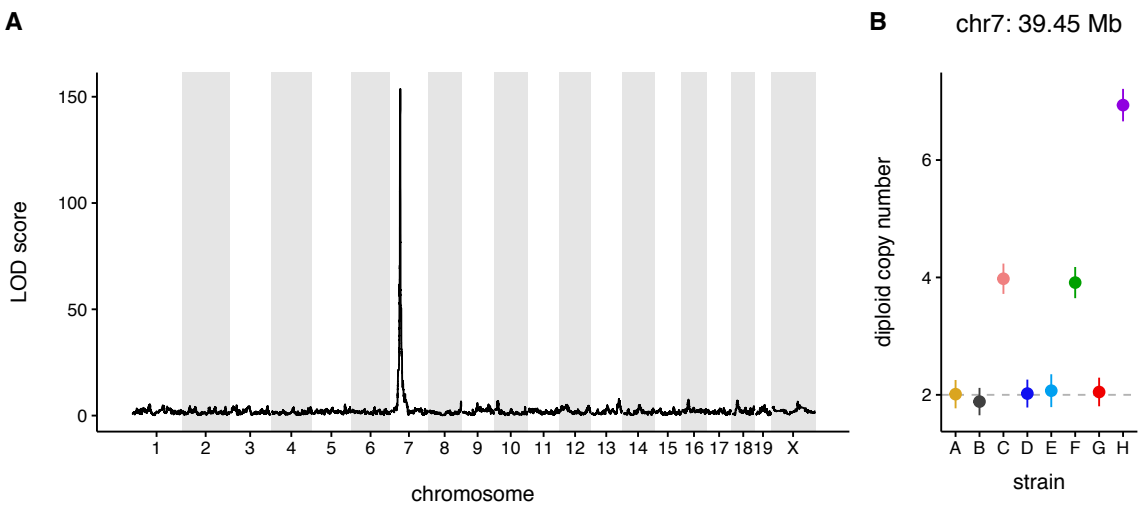

Figure S11: Genetic mapping confirms position and allelic configuration of complex CNVs. (**A**) LOD scores from single-locus QTL scan using copy number at chr7: 38.29 Mb as a quantitative trait. (**B**) Founder strain means (± 2 SE) at the QTL peak (chr7: 39.45 Mb), which provide a direct estimate of founder copy number at this triallelic CNV. Note that the QTL peak is not located exactly at the nominal position of the CNV.

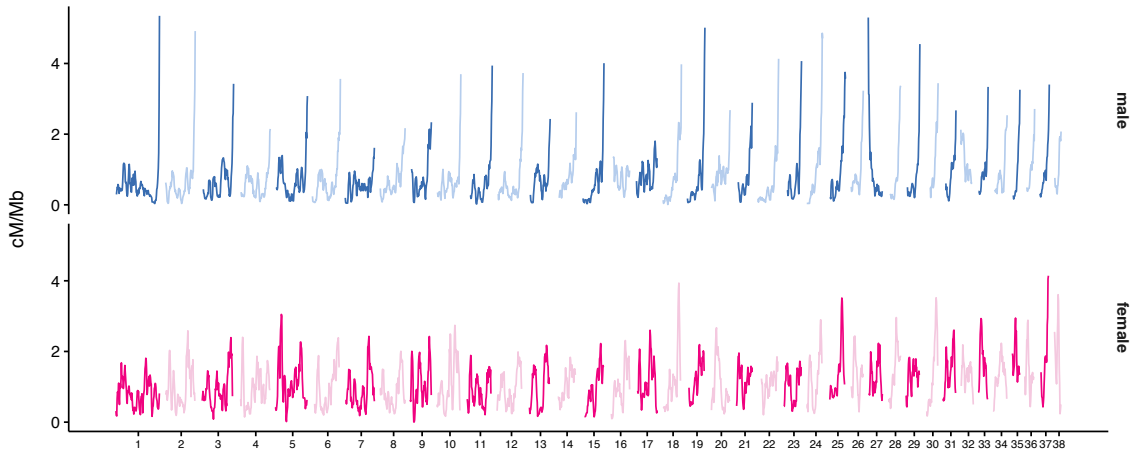

Figure S12: Sex-specific recombination rates in the domestic dog. Local sex-specific recombination rates (cM/Mb), calculated in 5 Mb windows with 1 Mb offset between adjacent windows, in a golden retriever pedigree Campbell *et al.* (2016). Note that the orientation of chromosomes 27 and 32 appear to be reversed with respect to the centromere.

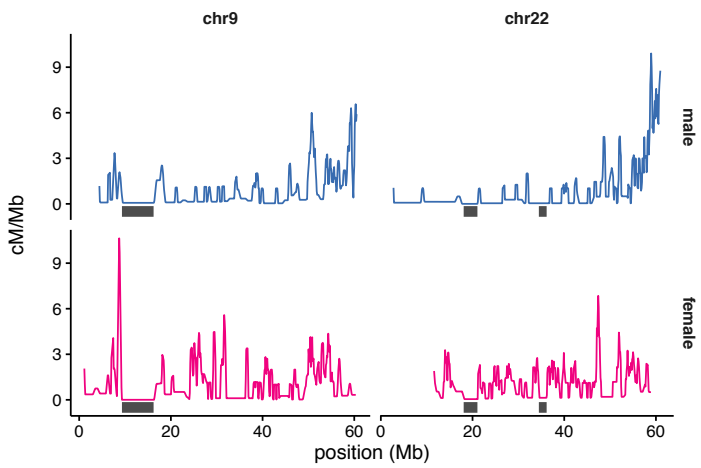

Figure S13: Recombination coldspots in the domestic dog. Local sex-specific recombination rates (cM/Mb), calculated in 500 kb windows, on portions of dog chromosomes 9 and 22. Coldspots ascertained on the sex-averaged map are indicated by grey bars along the x-axis. Due to variation in the distribution of informative markers in the pedigree, male and female maps do not necessarily cover the same genomic territory.

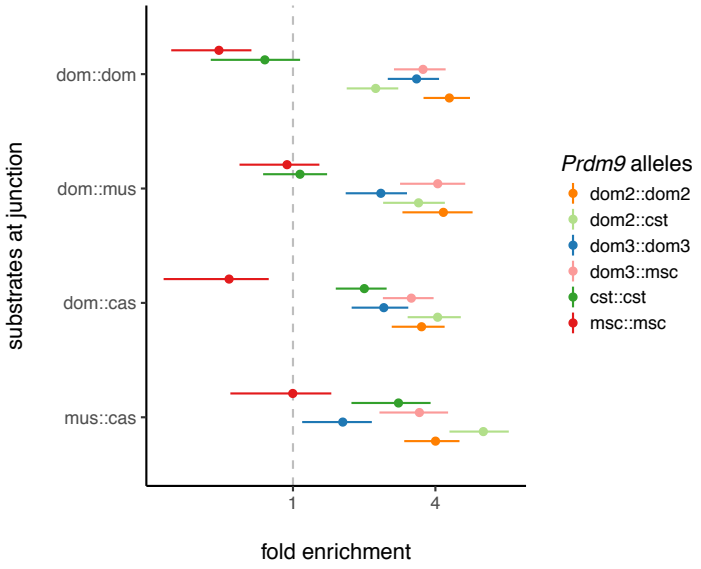

Figure S14: Enrichment of crossover intervals, stratified by local ancestry of the flanking haplotypes, for hotspots ascertained in the context of different *Prdm9* alleles.